Molecular Biology of the Cell
Vol. 15, 827–837, February 2004

Telomere Attachment, Meiotic Chromosome Condensation, Pairing, and Bouquet Stage Duration Are Modified in Spermatocytes Lacking Axial Elements

Bodo Liebe,*¶ Manfred Alsheimer,†¶ Christer Höög,‡ Ricardo Benavente,† and Harry Scherthan*§

*Max-Planck-Institut für Molekulare Genetik, D-14195 Berlin, Germany; †Department of Cell and Developmental Biology, Biocenter, University of Würzburg, D-97074 Würzburg, Germany; and ‡Department of Cell and Molecular Biology, Karolinska Institute, Stockholm, Sweden

Submitted July 24, 2003; Revised October 24, 2003; Accepted October 24, 2003
Monitoring Editor: Tim Stearns

During the extended prophase to the meiosis I division, chromosomes assemble axial elements (AE) along replicated sister chromatids whose ends attach to the inner nuclear membrane (NM) via a specialized conical thickening. Here, we show at the EM level that in *Sycp3*$^{-/-}$ spermatocyte chromosomes lack the AE and the conical end thickening, but still they attach their telomeres to the inner NM with an electron-dense plate that contains T_2AG_3 repeats. Immunofluorescence detected telomere proteins, SCP2, and the meiosis-specific cohesin STAG3 at the *Sycp3*$^{-/-}$ telomere. Bouquet stage spermatocytes were approximately threefold enriched, and the number of telomere but not centromere signals was reduced to the haploid in advanced *Sycp3*$^{-/-}$ spermatocytes, which indicates a special mode of homolog pairing at the mammalian telomere. Fluorescence in situ hybridization with mouse chromosome 8- and 12-specific subsatellite probes uncovered reduced levels of regional homolog pairing, whereas painting of chromosomes 13 revealed partial or complete juxtapositioning of homologs; however, condensation of *Sycp3*$^{-/-}$ bivalents was defective. Electron microscopic analysis of AE-deficient spermatocytes revealed that transverse filaments formed short structures reminiscent of the synaptonemal complex central region, which likely mediate stable homolog pairing. It appears that the AE is required for chromosome condensation, rapid exit from the bouquet stage, and fine-tuning of homolog pairing.

INTRODUCTION

Meiosis is essential for sexual reproduction in that it enables the independent assortment of homologous chromosomes (homologs) and the reduction of chromosome number to the haploid. To this end, homologs pair and establish stable connections during an extended prophase that precedes the reductional meiosis I division (MI). A subsequent second division (MII) separates sister chromatids, leading to formation of haploid gametes or spores. Before pairing of homologs at prophase I, these extend and attach their ends (telomeres) to the nuclear envelope. Concomitantly with this change in nuclear architecture, protein axes (axial elements; AEs) are formed along replicated sister chromatids (leptotene). Subsequently, chromosomes move and initiate stable pairing between them (zygotene) by assembly of proteinaceous transverse filaments between AEs (now called lateral elements; LEs), which forms the synaptonemal complex (SC) that connects all homologs at pachytene (von Wettstein *et al*., 1984; Hunter, 2003).

AEs contain SCP3 and SCP2 proteins that assemble on cohesin cores that are laid down during premeiotic S phase (Prieto *et al*., 2001; Eijpe *et al*., 2003). Resolution of sister chromatid cohesion, first between chromatids during MI and subsequently between sister centromeres during the meiosis II division, allows chromosome reduction (Buonomo *et al*., 2000; for reviews, see Lee and Orr-Weaver, 2001; Petronczki *et al*., 2003). These processes have evolved by addition of meiosis-specific components to the cohesin complex. In mammals, for instance, STAG3 (an ortholog of Smc3, Rec11, AS1,2; Pezzi *et al*., 2000; Prieto *et al*., 2001) and SMC1β constitute meiosis-specific cohesins (Revenkova *et al*., 2001). Furthermore, the conserved meiosis-specific Rec8 cohesin locates to meiotic cohesin cores and is required for AEs and SC assembly and recombination (Molnar *et al*., 1995; Klein *et al*., 1999; Watanabe and Nurse, 1999; Eijpe *et al*., 2003).

The cohesin cores that form during meiosis seem to provide a scaffold for the binding of AE and recombination proteins (Pelttari *et al*., 2001; Eijpe *et al*., 2003). In mammalian meiosis, cohesins have been found to interact with the AE proteins SCP2 and SCP3 (Eijpe *et al*., 2000, 2003), the latter of which is required for formation of silver-staining AEs (Yuan *et al*., 2000). The ends of AEs (telomeres) attach to the meiotic nuclear envelope during early leptotene, where they move to cluster at the leptotene/zygotene transition (known as bouquet formation) (von Wettstein *et al*., 1984; Zickler and Kleckner, 1998; Scherthan, 2001).

Telomeres are DNA/protein complexes at chromosome ends that contribute to chromosome and genome stability

Article published online ahead of print. Mol. Biol. Cell 10.1091/mbc.E03–07–0524. Article and publication date are available at www.molbiolcell.org/cgi/doi/mbc.E03–07–0524.

¶ These authors contributed equally to the work.
§ Corresponding author. E-mail address: schertha@molgen.mpg.de.

(for review, see McEachern *et al*., 2000; de Lange 2002). Meiotic telomeres consist of duplex $(T_2AG_3)_n$ repeats that are bound by TRF1, TRF2, and associated proteins (Scherthan *et al*., 2000a). TRF2 shares homology with the Taz1 telomere protein of *Schizosaccharomyces pombe* (Li *et al*., 2000), which is essential to meiotic telomere clustering (Cooper *et al*., 1998; Nimmo *et al*., 1998). A minimal set of telomere repeats (Naito *et al*., 1998; Maddar *et al*., 2001) and telomeric repeat binding factor proteins such as Taz1 and its interacting protein spRap1 are required for tethering telomeres to the spindle pole body (the yeast MTOC) in the nuclear envelope of fission yeast meiocytes (Chikashige and Hiraoka, 2001; Kanoh and Ishikawa, 2001).

The ends of mammalian AEs attach with the wide end of a conical thickening to the inner nuclear membrane (Woollam *et al*., 1966; Esponda and Giménez-Martín, 1972; Holm and Rasmussen, 1977). Proteins involved in the formation of this conical AE end and its attachment to the inner nuclear membrane are speculative. Previously, disruption of the gene coding for synaptonemal complex protein 3 (*Sycp3*, also known as *SCP3*; Lammers *et al*., 1994; Yuan *et al*., 1998) has been found to obstruct formation of silver-positive AEs and SCs and to induce cell death of mutant spermatocytes during an extended zygotene stage (Yuan *et al*., 2000). In female meiosis, SCP3 and the AE is dispensable for homolog pairing but is required for ordered crossover distribution (Yuan *et al*., 2002). Thus, SCP3 seems to be a major determinant of meiotic chromosome structure and may play a role in crossover control.

Here, we made use of SCP3-deficient spermatogenesis and investigated by molecular cytology and electron microscopy (EM) the role of the AE and its major protein component SCP3 in telomere dynamics, ultrastructure, nuclear envelope (NE) attachment, meiotic chromosome structure, and homolog pairing throughout prophase I in the male mouse.

MATERIALS AND METHODS

Testicular Specimens and Preparation

Mouse spermatocytes were obtained from C57BL/6 mice and from *Sycp3*$^{-/-}$ mice that were generated in the same background (Yuan *et al*., 2000). Animals were anesthetized and sacrificed by cervical dislocation. Testes were immediately resected and shock frozen for 5 min in 2-methyl-butane (Sigma-Aldrich, St. Louis, MO) at −70°C and stored at −80°C in the presence of 2-methyl-butane until further use.

Structurally preserved nuclei for simultaneous SC-immunostaining and fluorescence in situ hybridization (FISH) were prepared by mincing fresh or frozen testicular tissue in MEM (Invitrogen, Carlsbad, CA)/0.5% mammalian protease inhibitor (Sigma-Aldrich) at 4°C. After removal of tissue pieces, a drop of the suspension was placed on clean aminosilane-coated glass slides and immediately mixed with two drops of fixative (3.7% formaldehyde, 0.1 M sucrose, phosphate-buffered saline [PBS], pH 7.4). After air-drying at 4°C, slides were stored at −20°C until further use. Swab preparations were obtained as described previously (Scherthan *et al*., 2000a).

Detergent spreading of spermatocytes was based on the protocols of Peters *et al*., (1997) and (Scherthan *et al*., 2000a) with the following modifications: ~10 μl of a testicular suspension was placed on a glass slide and mixed gently with 80 μl of ionic detergent solution 1% Lipsol (LIP, Shipley, United Kingdom). Swelling/spreading of spermatocytes was allowed for ~10 min followed by addition of 90 μl of fresh fixative solution (1% p-formaldehyde, 10% 50 mM $NaBH_3$, pH 9.2, 0.15% Triton X-100, pH 9.2) and gentle tilting. Slides were dried for 2 h in a humid chamber, washed three times with 0.1% Agepon (Agfa, Cologne, Germany), and stored at −70°C until further use.

Antisera

The following affinity-purified antibodies were used in the immunostaining experiments: telomere antibodies (kindly provided by T. de Lange (Rockefeller University, New York, NY), rabbit anti-mouse-TRF1 antisera (#644; J. Karlseder and T. deLange, unpublished data); TRF2, rabbit anti-TRF2 antibodies #647 (Zhu *et al*., 2000); mRAP1, rabbit anti-human-Rap1 antiserum (#765; Li *et al*., 2000); SCP1, rabbit anti-SCP1 antiserum (Liu *et al*., 1996); rabbit anti-SCP2 antiserum (Offenberg *et al*., 1998; kind gift of C. Heyting) (Wageningen University, the Netherlands); SCP3, guinea pig anti-SCP3 antiserum (Alsheimer and Benavente, 1996); a monoclonal antibody to γ-tubulin (Sigma-Aldrich). Rabbit α-STAG3, a meiosis-specific cohesin (Pezzi *et al*., 2000), was kindly provided by J. Barbero (UAM, Madrid, Spain). An antiserum to testis-specific histone H1t (Moens, 1995) was kindly provided by P. Moens (York University, York, ON, Canada). All antisera were used at 1/1000 dilution in PBTG (PBS, 0.05%Tween 20, 0.2% bovine serum albumin, 0.1% gelatin), except for STAG3 that was used at 1:500. All antibodies were tested in individual staining reactions for their specificity and performance. Secondary antibodies to the primary ones with different fluorochromes were from commercial suppliers (Scherthan *et al*., 2000a). Controls without primary and secondary antibodies were all negative (our unpublished data).

Immunofluorescence Staining

Fresh or frozen preparations (see above) were rinsed in water and then in PBS/0.1% glycine to remove sucrose and formaldehyde. Immunofluorescence (IF) staining was done as published in Scherthan *et al*. (2000). Preparations were mounted in antifade solution (Vectashield; Vector Laboratories, Burlingame, CA) containing 0.5 μg/ml 4,6-diamidino-2-phenylindole (DAPI) (Sigma-Aldrich) to reveal nuclear DNA. In mouse testicular suspension preparations, the stage-specific distribution of SCP1 proteins and/or DAPI-bright heterochromatin clusters was used to identify spermatocytes at various stages of prophase I (Scherthan *et al*., 1996).

Because SC and anti-telomere protein antisera used were in many cases derived in rabbits, all costaining reactions were performed consecutively with and without axial element detection. All IF reactions were carried out in parallel on structurally preserved and swab preparation testicular nuclei (Scherthan *et al*., 2000a) and on spreads (see above). When two rabbit antisera were used in one experiment, the staining reactions were carried out sequentially with an intervening incubation with unlabeled anti-rabbit Fab fragments (Dianova, Hamburg, Germany) and a 1-min fixation in 1% formaldehyde/PBS to mask all rabbit epitopes and eliminate cross-reactivity.

Electron Microscopy

Testes were fixed in 2.5% cacodylate-buffered glutaraldehyde (1 h, 4°C) and then postfixed with 1% osmium tetroxide (1 h). After overnight staining with 0.5% uranyl acetate, testes were dehydrated in ethanol series and embedded in Epon. Ultrathin sections were double stained with uranyl acetate and lead citrate. Alternatively, testes were fixed in PBS-buffered formaldehyde (4%, 1 h) and embedded in RL White according to standard procedures. For control by light microscopy, semithin sections were prepared from embedded testes and stained with 1% toluidine blue. Micrographs were obtained with an EM-10 electron microscope (Carl Zeiss, Jena, Germany).

EM-In Situ Hybridization (ISH)

For EM-ISH ultrathin sections of LR White-embedded testes were transferred to Formvar-coated nickel grids. Sections were pretreated for 1 h at 37°C with RNase A (100 μg/ml in 2× SSC), washed twice in 2× SSC for 5 min, and incubated with 0.5 mg/ml OB-Protease (PeqLab, Erlangen, Germany) in 20 mM Tris-HCl, 2 mM $CaCl_2$ (pH 7.4) for 8 min at room temperature, followed by two 5-min washes in 2× SSC. After 20-min denaturation in hybridization solution (30% formamide, 10% dextransulfate, 250 μg/ml *Escherichia coli* genomic DNA in 2× SSC) at 93°C, samples were hybridized in the presence of Dig-labeled $(T_2AG_3)_7/(C_3TA_2)_7$ oligomeres (0.5 pmol/μl each) for at least 18 h at 37°C. Grids were rinsed 2 × 10 min in 2× SSC at 37°C and after 30-min blocking with 0.5% Blocking-Reagent (BR, Roche Diagnostics, Mannheim, Germany) in Tris-buffered saline (TBS) (TBS/BR) incubated with mouse anti-Dig-antibodies (Roche Diagnostics; 1:20 in TBS/BR) for 1 h. Subsequent washing was done twice in TBS containing 0.05% Tween 20 (TBST) and samples were incubated 1 h with secondary antibody (goat anti-mouse coupled with 12-nm gold; Dianova) diluted 1:7.5 in TBS/BR. Sections were washed twice in TBST for 10 min, rinsed 2 × 5 min in H_2O, and air dried. Contrasting was done according to standard protocols.

DNA Immunodetection by the Terminal Deoxynucleotidyl Transferase Method

The 3′ DNA ends generated by tissue sectioning of LR White embedded testes were extended by a terminal transferase reaction by using nucleotides and Dig(Digoxigenin-II)dUTP as described by Thiry (1992). The incorporated Dig-dUTP molecules were then immunodetected with primary anti-Dig antibodies (Roche Diagnostics) and secondary antibodies conjugated with 12-nm gold particles (Dianova, Hamburg, Germany).

DNA Probes and Labeling

Mouse chromosome 8- and 12-specific, repetitive subsatellite DNA clones (Boyle and Ward, 1992) were used to tag the respective chromosomes (Scherthan *et al*., 1996). An MMU 13-specific paint probe was obtained from Cambio (Cambridge, United Kingdom). A Cy5-labeled 42mer deoxynucleotide oligomer homologous to the pericentromeric mouse major satellite DNA was used to probe for centromeric heterochromatin (Scherthan *et al*., 1996). Biotin-labeled $(TTAGGG)_7/(CCCTAA)_7$ oligomeres were used to illuminate mouse

telomeres. Specificity of oligomeres was confirmed by FISH to metaphase chromosomes (our unpublished data). The labeling of the oligomeres by terminal tailing and of the plasmid DNA by Nick translation was carried out as described previously (Scherthan *et al*., 1996).

IF-FISH

Combinatorial immunostaining and FISH was carried out as described (Scherthan *et al*., 1996). Briefly, SCP1 protein was first immunostained using a rabbit anti-SCP1 antiserum (Yuan *et al*., 1998) and visualized by binding of a secondary α-rabbit-Cy5–labeled antibody (Jackson ImmunoResearch Laboratories, West Grove, PA) followed by a fixation for 5 min in 1% formaldehyde/PBS. Preparations were then denatured in the presence of DNA probes and hybridized for 12 h at 37°C, followed by three 5-min washes in 0.05× SSC at 37°C. Hybrid molecules were detected using biotin/avidin-Cy3 (Vector Laboratories) and anti-digoxygenin rhodamine (Roche Diagnostics) as described previously (Scherthan *et al*., 1996). Preparations were finally embedded in antifade (Vector Laboratories) containing 0.5 μg/ml DAPI as DNA counterstain and analyzed in the microscope.

Microscopic Evaluation

Preparations were evaluated using an Axioskop epifluorescence microscope (Carl Zeiss) equipped with single-band pass filters for excitation of green, red, blue, and infrared, and a double-band pass filter for simultaneous excitation of red and green fluorescence (Chroma Technology, Brattleboro, VT) and 63× and 100× Plan-Neofluar lenses. Digital black-and-white images were recorded with a cooled charge-coupled device camera (Hamamatsu Photonics, Hamamatsu City, Japan) and merged to RGB-images by the ISIS fluorescence image analysis system (MetaSystems, Altlusshein, Germany). Images were further processed using Adobe Photoshop to match the fluorescence intensity seen in the microscope.

Three-dimensional evaluation of immunostained nuclei was performed in some experiments by using an Axioskop epifluorescence microscope (Carl Zeiss) equipped with a 100× Plan-Neofluar oil-immersion lens (numerical aperture 1.35; Carl Zeiss) attached to a PIFOC z-SCAN (Physik Instrumente, Waldbronn, Germany) and a 12-bit charge-coupled device digital camera (PCO; SensiCam, Kelheim, Germany) controlled by the TILLvisION 4.0 software. Fluorochromes were excited using a polychrome IV monochromator (TILL Photonics, Martinsried, Germany) in combination with a quadruple-band pass beam splitter and barrier filter (Chroma Technology), allowing subsequent excitation and recording of blue (DAPI), red (Cy3), green (fluorescein isothiocyanate, FITC), and infrared (Cy5) fluorescence in the same focal plane. Fluorescence profiles were derived from gray scale pixels values along interactively determined polygon tracks in raw digital-RGB images by using the Line Profile measurement option of the TILLvisION software. Deconvolution was carried out on 0.2-μm–spaced image stacks by using the cMLE algorithm of Huygens2.1.4-essential (Scientific Volume Imaging) running under Windows-NT. Rendering of three-dimensional data was done using the Surpass module of Imaris3.3.2 (Bitplane, Basel, CH).

RESULTS

The SCP3 protein represents a major component of the axial element that attaches to the inner nuclear membrane (NM) with an electron-dense conical thickening that is conserved among kingdoms (Moens, 1969; Esponda and Giménez-Martín, 1972; Holm, 1977). To see whether SCP3 and the AE are required for telomere attachment and dynamics during mouse meiosis, we performed FISH with PNA probes to $(T_2AG_3)_n$ repeats in combination with IF staining of one of the following: the STAG3 meiotic cohesin, the SCP2 AE protein, or the SCP1 transverse filament SC protein. FISH IF staining of structurally preserved nuclei obtained from *Sycp3*$^{-/-}$ testes suspensions revealed SCP1 fibers as well as foci of SCP2 protein in knock-out spermatocytes (see below), which agrees with previous analysis (Yuan *et al*., 2000; Pelttari *et al*., 2001).

Three-dimensional fluorescence microscopy of structurally preserved spermatocyte nuclei showed that telomeres are dispersed throughout premeiotic mutant and wild-type nuclei (n = 25 each; not shown). Telomeres obtained an exclusively peripheral position from leptotene up to pachytene in the wild type, and in leptotene up to advanced zygotene-like *Sycp3*-mutant nuclei (Figure 1). The latter were identified by the presence of short and long STAG3 fibers (Figure 1) or by SCP1 fiber fragments (see below; Yuan *et al*., 2000; Pelttari *et al*., 2001). Furthermore, immunostaining of the testes-specific histone H1t (see Scherthan *et al*., 2000b for details) showed the absence of this pachytene marker in *Sycp3*$^{-/-}$ spermatocytes (our unpublished data). Because H1t fluorescence is seen only after chromosome pairing is complete (Moens 1995), the absence of H1t expression agrees with arrest of *Sycp3*$^{-/-}$ spermatogenesis in a zygotene-like stage (Yuan *et al*., 2000).

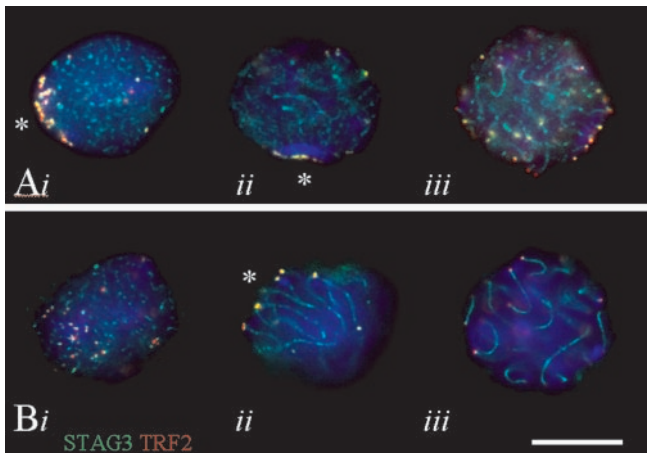

Figure 1. Immunofluorescence staining of cohesin cores (STAG3, green) and telomeres (TRF2, red) in structurally preserved (A) *Sycp3*$^{-/-}$ and (B) *Sycp3*$^{+/+}$ spermatocytes I. (Ai) *Sycp3*$^{-/-}$ leptotene nucleus with a tight telomere cluster at a sector of the nuclear periphery (*) and STAG3 cohesin speckles (all focal planes in A at nuclear equator). (Aii) *Sycp3*$^{-/-}$ zygotene nucleus with STAG3 speckles and cores; telomeres are clustered at a limited sector of the NE (*). (Aiii) Advanced *Sycp3*$^{-/-}$ zygotene nucleus with STAG3 cores and telomeres dispersed about the nuclear periphery. (Bi) Wild-type leptotene nucleus with numerous STAG3 speckles and most telomeres accumulated at the lower left of the nuclear top. (Bii) Late wild-type zygotene nucleus with long STAG3 cores and telomeres clustered at a limited sector of the NE (zygotene bouquet; *, focal plane at nuclear equator). (Biii) Wild-type pachytene nucleus with synapsed STAG3 cohesin cores and telomeres dispersed about the nuclear periphery (focus at nuclear equator). Nuclear DNA was revealed with DAPI (blue). Note that telomere clustering is tighter in the *Sycp3* mutant. Bar (B): 10 μm; it applies to all details.

Morphogenesis of the Chromosome End Is Altered in the Absence of SCP3

To study the nature of telomere attachment in the absence of SCP3 and the AE at a higher resolution, we performed transmission EM of wild-type and *Sycp3*$^{-/-}$ spermatocytes from testes tissue sections using a random section approach. Wild-type SCs displayed the typical conical LE thickening at the LE/NE attachment (Figure 2A). The AE attachment of *Sycp3*$^{-/-}$ spermatocytes differed remarkably: the electron-dense end of the AE core with its prominent conical thickening was missing in the *Sycp3* mutant, whereas a disk-shaped electron-dense plate of ~200 nm in diameter was intimately associated with the nuclear face of the inner nuclear membrane (Figure 2, B–F). At proximal telomeres we often observed a stalk between the disk-shaped attachment plate at the inner nuclear membrane and the bulk of the adjacent heterochromatin (Figure 2, B–D). This is reminiscent of the ultrastructure of the proximal chromosome end in wild-type mouse spermatocytes (Stack, 1984). At distal telomeres, the *Sycp3*$^{-/-}$ attachment plate formed a flat electron-dense structure with the adjunct chromatin being unstructured (Figure 2, E and F).

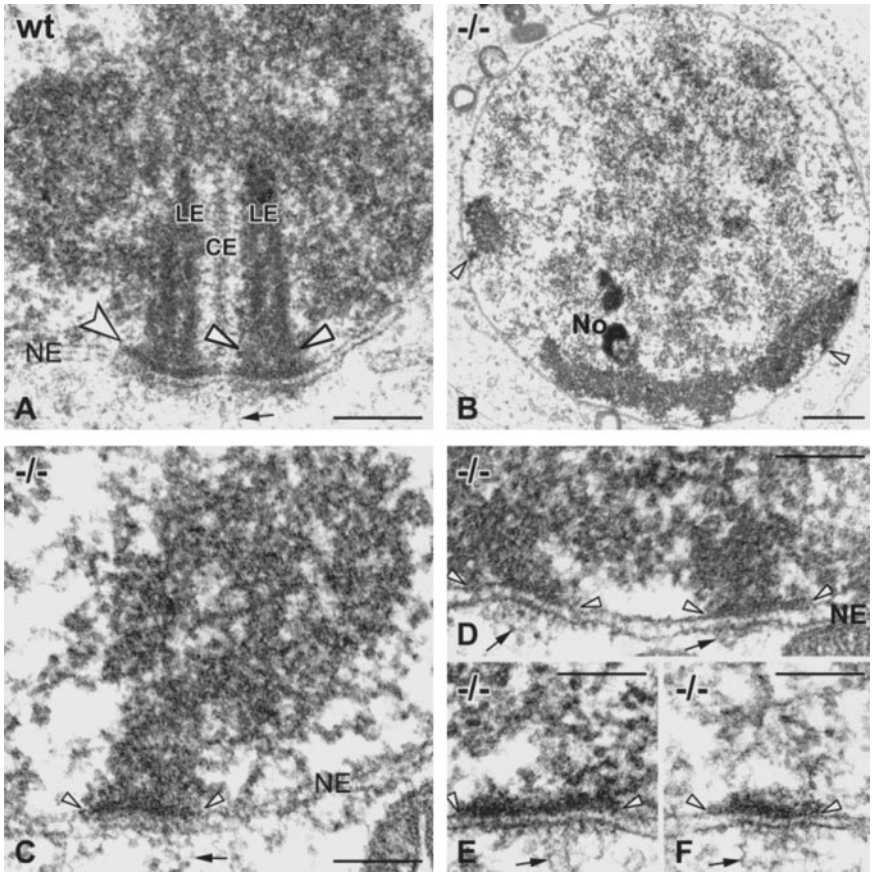

Figure 2. EM of telomere attachments in *Sycp3*$^{+/+}$ (A) and *Sycp3*$^{-/-}$ spermatocytes (B–F). (A) Electron-dense LEs of the SC (CE, central element) terminate with a conical thickening (arrowheads) at the inner NM of a wild-type (WT) spermatocyte I nucleus. An electron-dense plate connects the wide end of the LE thickening with the inner NM (indented arrow). Note: the double-stranded nature of the LEs was only seen in this preparation but is known from hamster LEs (Dresser and Moses, 1980). (B) Overview of a *Sycp3*$^{-/-}$ bouquet spermatocyte at the leptotene/zygotene transition as indicated by the clustered, electron-dense heterochromatin in the lower region of the nucleus. Several telomere attachment plates are seen (arrowheads; No, nucleolus). (C and D) Details of *Sycp3*$^{-/-}$ attachment plates of proximal telomeres at the inner NM (demarcated by arrowheads). A stalk of dense chromatin extends from the adjacent bulk heterochromatin to the nuclear envelope and terminates in a flat electron-dense attachment plate (arrowheads). (D) Two telomere attachment plates that are ~330 nm apart. (E and F) Distal telomere attachments (without adjacent heterochromatin) show solely an electron-dense plate at the nucleoplasmic face of the inner NM with the adjunct chromatin being unstructured. Fibrillar material spanning the nuclear envelope emanates into the cytoplasm opposite of all telomere attachments (small arrows). Bars (A, C–F) 0.2 μm; (B) 2 μm.

Furthermore, we observed fibrillar material that extended from the attachment plate through the NE and emanated into the cytoplasm in wild-type and *Sycp3*$^{-/-}$ spermatocytes (Figure 2). These filaments are of 4–5 nm in diameter and have been observed at zygotene and pachytene telomeres in other species, but their function and composition have remained obscure (Esponda and Giménez-Martín, 1972; Holm, 1977; Bojko, 1990; Benavente *et al*., 2004). Together, our EM analysis suggests that the SCP3 protein be the major component of the conical thickening of the AEs/LEs adjacent to the telomere attachment plate at the inner nuclear membrane.

Attachment Plates Contain Telomere Sequences

Information about specific nucleic acids contained in the telomere attachment plate is scarce (Esponda and Giménez-Martín, 1972; Scherthan *et al*., 1996; Franco *et al*., 2002). We thus made use of the clear appearance of the attachment plate in *Sycp3*$^{-/-}$ spermatocytes and labeled DNA in ultrathin testes sections to investigate the presence of DNA and telomere repeats in this structure. After terminal transferase/digoxigenin-dUTP labeling, DNA-specific gold label was exclusively distributed over the nuclear chromatin and the attachment plates at the inner NM (Figure 3A) revealing the presence of DNA in the attachment plate. Next, EM-ISH with digoxygenin-labeled T_2AG_3 repeat probes disclosed telomere repeat-specific gold grains exclusively at the attachment plate at the nucleoplasmic face of the inner NM (Figure 3, B–D). The somewhat low density of gold grains obtained may result from a reduced labeling density generally obtained by EM-ISH to telomere repeats (Steinmüller *et*

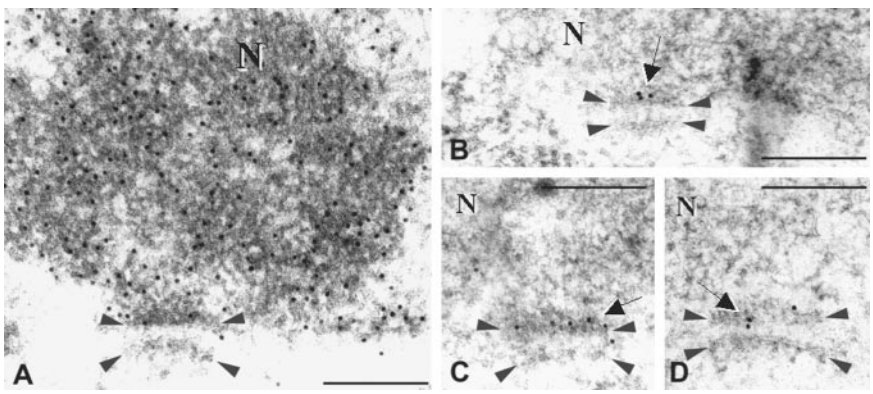

Figure 3. In situ DNA end labeling of *Sycp3*$^{-/-}$ nuclear sections (A) reveals DNA-specific gold grains over a detail of a spermatocyte I nucleus (N), which includes the attachment plates (demarcated by arrow heads). (B–D) Details of telomere attachments after EM-ISH with T_2AG_3 repeat probes. Specific telomere-repeat signals (black gold grains; arrows) are located exclusively at the attachment plates at the inner nuclear membrane (upper arrowheads), indicating that telomere repeats are contained in the attachment plate. This type of treatment also revealed an electron-dense "plate" at the cytoplasmic face of the NE, which was a particularity of EM-ISH and may represent a technical artifact due to collapse of the cytoplasmic fibrils opposite the telomere attachment at the inner NE. Bars, 0.2 μm.

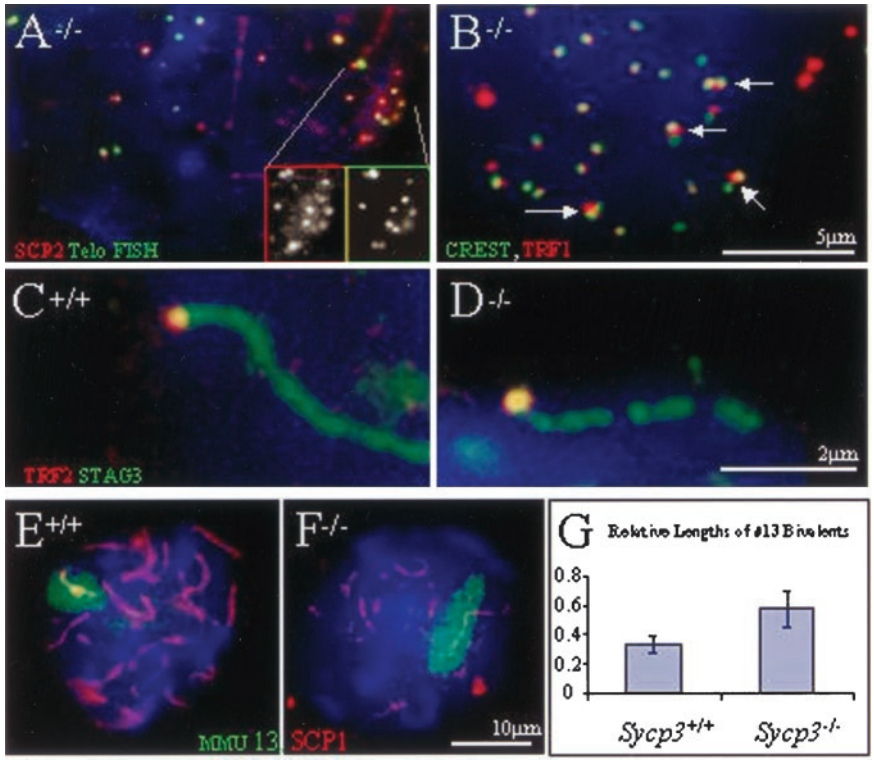

Figure 4. (**A**) SCP2 (green, FITC) and telomeres (red, T_2AG_3 FISH) colocalize in a *Sycp3*$^{-/-}$ spermatocyte. The detail shows the gray channels of the enlarged region. Colors for SCP2 protein and telomeres as indicated. (B) Telomere (TRF1 red) and kinetochore staining (CREST, green) in a *Sycp3*$^{-/-}$ spermatocyte. Several separated centromere signals have a common telomere signal between them (arrows). Note the increased telomere signal size at CREST signal doublets, which indicates pairing of telomeres. Bar, 5 μm. (C and D) Integrity of cohesin cores as determined in three-dimensionally preserved nuclei. (C) Wild-type telomere with a continuous cohesin core in its vicinity. (D) Detail of a *Sycp3*$^{-/-}$ cohesin core (STAG3, green) that has several disruptions in the vicinity of the associated telomere signal (TRF2, red). Bar, 2 μm. (E and F) SCP1 staining (red, Cy3) and painting of mouse chromosomes MMU13 (green, FITC). (E) A single MMU13 FISH signal delineates a MMU13 bivalent associated with a central SCP1 fiber in a wild-type spermatocyte. (F) An advanced *Sycp3*$^{-/-}$ spermatocyte displays an extended paint signal representing the MMU13 bivalent that contains a long interrupted SCP1 fiber along its center. (G) *Sycp3*$^{-/-}$ MMU13 bivalents are more extended than wild-type bivalents. The graph is based on the length of MMU13 bivalents from 20 wild-type pachytene and *Sycp3*$^{-/-}$ nuclei (MMU13 homologs were requested to be completely paired in the mutant to allow comparison with the wild-type bivalents). The bivalent length is expressed as the fraction of the maximal nuclear diameter (set to 1), as determined from its DAPI outline (blue). It is apparent that condensation of MMU13 bivalents is defective in the *Sycp3*$^{-/-}$ knockout, the difference being highly significant (t test, $p < 0.001$).

al., 1993). Interestingly, the EM-ISH pretreatment also revealed an electron-dense plate at the cytoplasmic face of the NE (Figure 3, A–D) where cytoplasmic filaments emanated that did not contain T_2AG_3-specific gold grains (Figure 3). It is likely that the dense appearance of the cytoplasmic plate may be the result of EM-ISH–induced collapse of the filaments at the cytoplasmic face of the outer NM, which agrees with the absence of an outer plate in EM investigations using other preparation techniques (Esponda and Giménez-Martín, 1972; Holm and Rasmussen 1977). Together, it seems that SCP3 is dispensable for the morphogenesis of flat telomere attachment at the inner NM.

Meiotic Cohesin Cores Are Capped by Telomere Proteins

To address the question whether the altered ultrastructure of the SCP3-deficient meiotic chromosome core affects the composition of the telomere complex, we performed two-color IF analysis with antibodies to TRF1, TRF2, and mammalian (m)RAP1 telomere proteins (Broccoli *et al*., 1997; Li *et al*., 2000) and the meiosis-specific STAG3 cohesin (Prieto *et al*., 2001), which delineates cohesin cores in *Sycp3*$^{-/-}$ spermatocytes (Pelttari *et al*., 2001).

Three-dimensional wide-field microscopy revealed that the ends of STAG3 cohesin cores located to the nuclear periphery and colocalized with all three telomere proteins investigated, namely, TRF1, TRF2, and mRap1 (Figures 1 and 4; our unpublished data) in wild-type and *Sycp3*$^{-/-}$spermatocytes. To test for the presence of meiotic cohesin proteins at the SCP3-deficient telomere, we performed fluorescence profile analysis (for details, see Scherthan *et al*., 2000a) and noted a perfect colocalization of STAG3 signals with all of TRF2-tagged telomeres in both genotypes (n = 105 in *Sycp3*$^{-/-}$ and n = 103 in the wild type). Furthermore, *Sycp3*$^{-/-}$ telomeres stained by a PNA telomere probe (n = 384) colocalized with 84% of short SCP2 fragments or dots (Figure 4A). In contrast, telomere/SCP1 colocalization was only seen at 13.4% of 715 SCP1 fibers (n = 715 derived from 50 *Sycp3*$^{-/-}$ nuclei that exhibited a mean of 14.3 SCP1 fibers/nucleus; not shown). This suggests that the meiotic telomere contains SCP2 and cohesin proteins but only rarely SCP1 transverse filament proteins. It is noteworthy that Yuan *et al*., (2002) noted the presence of distinct SCP2 dots of double the centromere number in *Sycp3*$^{-/-}$ oocytes. These numbers fit with the ~40 SCP2-positive telomere signals that were detected in *Sycp3*$^{-/-}$ spermatocytes and suggests that SCP2 also localizes to meiotic telomeres in the female.

The AE Is Required for Chromosome Condensation

Although the STAG3 cohesin was found at all *Sycp3*$^{-/-}$ telomeres, the STAG3 axes emanating from these telomeres often showed gaps within 0.7 μm off the TRF2-tagged telomeres in three-dimensional (3D)-preserved nuclei (Figure 4, C and D). This was the case in 33% of *Sycp3*$^{-/-}$ telomeres (n = 105), whereas only 3% of TRF2-tagged wild-type telomeres (n = 103) exhibited a disrupted STAG3 core within 0.7 μm (Figure 4D) (this extension was chosen because only few SCP3-deficient cohesin cores could be traced for >0.7 μm). Occasionally, short regions with weakly or no STAG3 fluorescence were observed along wild-type STAG3 cores, whereas in *Sycp3*$^{-/-}$ spermatocytes STAG3 cores seemed overall rugged and disrupted (Figure 1A). STAG3 signal loss could be due to local distension/instability of cohesin cores in the absence of SCP3.

To test whether rugged cohesion cores are an indication of defective chromosome condensation in male meiosis, we

painted homologous mouse chromosomes (MMU) 13 in spread *Sycp3*$^{-/-}$ and wild-type spermatocyte nuclei. We assumed that mutant spermatocytes I that displayed long SCP1 fibers and completely paired MMU13 paint signals have undergone homolog pairing in the absence of AEs and mature SC and are equivalent to pachytene in the wild type. We then determined the maximum extension of the MMU13 paint signal and compensated for variations in nuclear diameter by expressing MMU13 bivalent length as the fraction of the maximal nuclear diameter to reveal the state of bivalent condensation in both genotypes. It was found that *Sycp3*$^{-/-}$ MMU 13 bivalents (n = 20) were approximately 2 times the relative length of wild-type pachytene bivalents (Figure 4, E–G), with the differences being highly significant (t test, $p < 0.001$). Fully paired *Sycp3*$^{-/-}$ MMU 13 paint signals displayed fragments of SCP1 fibers along their length, which makes it likely that deposition of SCP3 contributes to the condensation of the AE and, consequently, the SC. An approximately twofold elongation of SCP1 fibers (SCs) in female *Sycp3*$^{-/-}$ pachytene bivalents (Yuan *et al*., 2002) makes it unlikely that the lack of condensation relates to demise of spermatocytes in an advanced zygotene-like stage.

Different Modes of Telomere and Centromere Association Are Revealed by the Absence of SCP3

To test for the quality of homolog pairing at telomeres and centromeres, we next determined the number of telomere signals in >90 wild-type pachytene and advanced *Sycp3*$^{-/-}$ spermatocyte nuclei by triple staining of TRF1, CREST, and SCP1 proteins. The evaluation of >3600 TRF1 signals/genotype revealed that in both genotypes spermatocytes displayed similar numbers of telomere signals, i.e., wild-type pachytene spermatocytes displayed a mean of 38.8 telomere signals/nucleus (±1.3 SD), whereas *Sycp3*$^{-/-}$ late zygotene-like spermatocytes with long SCP1 fibers contained an average of 40.9 telomere signals/nucleus (±3.8 SD). These data indicate a reduction of telomere number to the haploid during *Sycp3*$^{-/-}$ zygotene stage (41 telomere signals of 20 bivalents are expected upon homolog pairing—mind unpaired XY ends) and suggest that telomeres undergo homolog pairing in the absence of the AEs. However, the pairing of telomeres seems not to extend to adjacent centromeres, because CREST staining in advanced zygotene *Sycp3*$^{-/-}$ spermatocytes resulted in a mean of 30.3 centromere signals (SD 4.38, range 25–38), whereas a mean of 21.5 centromere signals (SD 0.98, range 20–23) was seen in 40 wild-type pachytene nuclei, the difference being highly significant (t test, $p < 0.001$).

Often, closely spaced pairs of centromeric CREST signals were associated with a single telomere signal (Figure 4B) in advanced *Sycp3*$^{-/-}$ zygotene nuclei, which suggests that meiotic telomeres become tightly paired, while the adjacent centromere signals may still be separated. This explains why there is more than the haploid number of centromere signals in *Sycp3*$^{-/-}$ spermatocytes (this study; Yuan *et al*., 2000). The disparity of *Sycp3*$^{-/-}$ telomere/centromere numbers may be due to a general lack of synapsis at zygotene pericentromeres, leading to separation of those centromeres that are connected by a short LE stalk to the proximal telomeres (Figure 2, B and C; Stack, 1984). Defective kinetochore cohesion may not contribute to this observation, because we always observed two opposed similar-sized kinetochore signals. Lack of sister chromatid cohesion would have created three or four signals; at meiosis each centromere consists of two tightly connected sister kinetochores.

The reduction of telomere number in SCP3-deficient meiosis suggests that pairing/cohesion at meiotic telomeres does not require SCP3 or SCP1 synaptonemal complex proteins (Meuwissen *et al*., 1992; Lammers *et al*., 1994), being consistent with the observation that the SCP1 IF signal only marginally overlapped with the dot-like IF signal of TRF1-stained telomeres in wild-type (WT) bivalents (our unpublished data).

Sycp3 Disruption Alters Telomere Clustering

We next addressed the question whether the pairing of telomere signals in *Sycp3* knockout spermatocytes could be mediated by meiotic telomere clustering (bouquet formation), which is thought to stimulate homolog interactions (for review, see Loidl, 1990; Scherthan, 2001). In male mouse meiosis, telomeres reposition to the NE during preleptotene, whereas telomere clustering (bouquet stage) occurs subsequently during a short time window at the leptotene/zygotene transition (Scherthan *et al*., 1996). Frequencies of midpreleptotene and bouquet-stage spermatocytes were determined in testes suspensions according to their specific major satellite DNA and telomere distribution patterns (Figure 5, A and B; Scherthan *et al*., 1996, 2000a), and similar frequencies for midpreleptotene spermatocytes but increased frequency of bouquet cells were observed between wild-type and the *Sycp3* knockout (Figure 5C). Two-color IF for γ-tubulin (a marker for the MTOC) and telomeres confirmed that the clustering of mouse telomeres occurred in the vicinity of the centrosome (Figure 5D). Compared with wild-type testis suspensions, which displayed a frequency of 0.8% bouquet spermatocytes (based on 2005 prophase I nuclei), *Sycp3*$^{-/-}$ testicular suspensions were 2.8-fold enriched in bouquet stage cells (2.2% of 2028 nuclei; Figure 5C) with the difference being highly significant (χ^2, $p < 0.001$). Tight telomere clustering already in leptotene spermatocytes (Figure 1A) and the accumulation of bouquet nuclei in the *Sycp3* mutant suggests that the disruption of the meiotic chromosome core alters telomere movements and leads to an extended duration of the bouquet stage.

SCP3-deficient Spermatocytes Retain a Potential for Homology Interactions

The transverse filament (TF) protein SCP1 forms fibers of irregular lengths in *Sycp3*-knockout spermatocytes (see above; Yuan *et al*., 2000; Pelttari *et al*., 2001). However, it remained unclear whether these fibers reflect regional homolog interactions or nonhomologous synapsis (Yuan *et al*., 2000). To test for regional homolog interactions, we performed FISH with two chromosome-specific DNA probes that highlight the subsatellite region of mouse chromosomes (MMU) 8 and 12 (Boyle and Ward 1992). Two-color FISH revealed paired homologous MMU8 or 12 signals in 4.2% of *Sycp3*$^{-/-}$ mutant and wild-type spermatogonia (n = 56 and 48, respectively). Nuclei with a speckled appearance of SCP1 signals (zygotene in both genotypes) displayed pairing of both MMU 8 and MMU12 signals in 84% of wild type nuclei but only in 7% of *Sycp3*$^{-/-}$ zygotene nuclei (Figure 6). Furthermore, 18% of *Sycp3*$^{-/-}$ zygotene nuclei showed MMU12 paired and MMU8 separate, whereas 11% had MMU8 signals paired and MMU12 separated.

In wild-type pachytene nuclei (n = 149), all MMU8 and 12 signals were homologously paired, whereas only 19% of advanced *Sycp3*$^{-/-}$ spermatocytes (n = 86), displayed pairing of both homologous MMU8 and 12 signals (Figure 6). Fourteen percent of *Sycp3*$^{-/-}$ spermatocytes contained paired MMU12 and separated MMU8 signals, whereas 11% contained paired MMU8 and separated MMU12 signals,

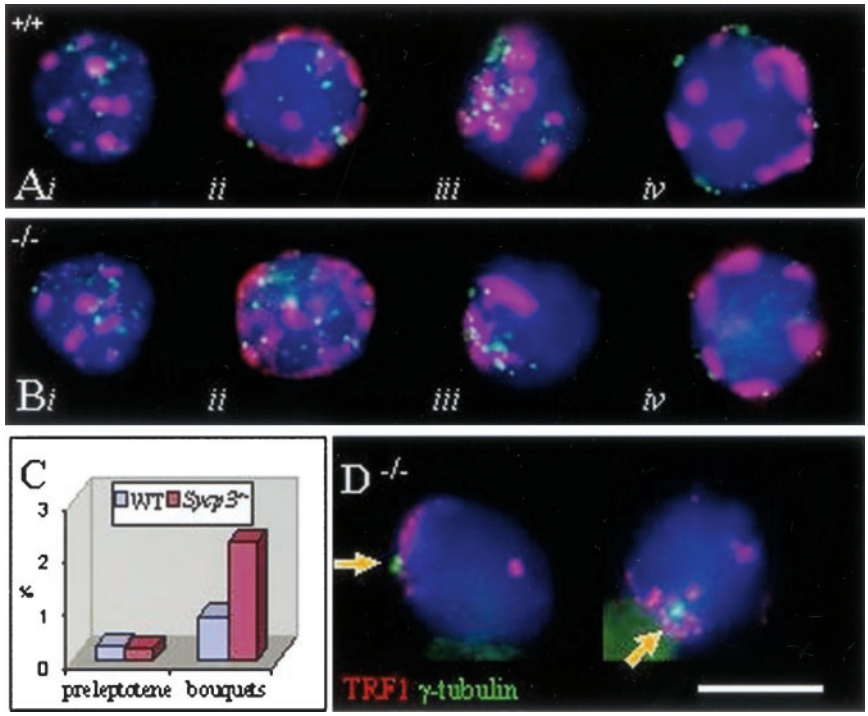

Figure 5. Telomere (green, T_2AG_3) and centromere (red, major sat.) FISH patterns in structurally preserved nuclei from *Sycp3*$^{-/-}$ and wild-type (*Sycp3*$^{+/+}$) testes suspensions. For staging according to FISH patterns, see Scherthan *et al.* (1996). (Ai and Bi) Premeiotic nuclei (blue, focal plane at nuclear equator) with numerous internal telomere and satellite DNA clusters. (Aii and Bii) Mid-preleptotene nuclei with peripheral satellite DNA and internal telomere signals (nuclear equator). (Aiii and Biii) Leptotene/zygotene nuclei (focal plane at nuclear top) with telomere clustering (bouquet topology). (Aiv) Wild-type pachytene and (Biv) advanced late zygotene *Sycp3*$^{-/-}$ nucleus with dispersed peripheral telomeres and satellite DNA clusters (focal plane at nuclear equator). Bar (B), 10 μm, it applies to all details. (C) Frequency of mid-preleptotene spermatocytes is similar in the wild-type and Sycp3 knockout, whereas bouquet frequency is 2.8-fold elevated (2.2%, n = 2028 nuclei) compared with the wild type (0.8%; n = 2005 nuclei), which is statistically highly significant (χ^2, $p < 0.001$). (D) Mouse telomeres (TRF1, red) cluster in the vicinity of the centrosome (arrow) as marked by γ-tubulin IF (green) in three-dimensionally preserved bouquet stage spermatocytes. Bar (D), 10 μm.

suggesting that homolog pairing is delayed in the *Sycp3* mutant and occurs on a chromosome-by-chromosome and regional basis. Higher numbers of paired signals for the smaller MMU12 chromosome are consistent with the idea that small chromosomes pair early in prophase I (see Scherthan and Schönborn, 2001, and references therein).

SCP1 Connects Homologous Sequences in the Absence of the AE

Triple-labeling of SCP1 by IF and MMU8, and MMU12 with region-specific FISH revealed colocalization of SCP1 fiber fragments and paired chromosome-specific FISH signals in 36% of paired MMU8 signals (n = 28) and in 29% of paired MMU12 signals (n = 28) (Figure 6, A and D), which indicates that a significant fraction of SCP1 fibers that form in *Sycp3*$^{-/-}$ spermatocytes connect homologous chromatin, whereas the majority of homologously paired MMU8 and 12 signals did not recruit SCP1.

When we determined overall homolog interactions by using a MMU 13-specific paint probe, it was found that 57% of advanced *Sycp3*$^{-/-}$ spermatocytes with long SCP1 fibers (n = 28) displayed a single painted MMU13 bivalent (Figure 4F), whereas in all the remaining advanced knockout spermatocytes chromosomes 13 were partially paired, being consistent with a zygotene arrest in the male *Sycp3*$^{-/-}$ mutant. In the wild-type all of 25 pachytene nuclei displayed a single MMU13 bivalent (Figure 4E). The meiosis-specific level of homolog pairing seen in SCP1-positive *Sycp3*$^{-/-}$ spermatocytes (Figures 4 and 6C) indicates that the AE is not required for stable homolog pairing and that a few sites of such interactions are sufficient to connect homologs.

A large fraction of separate region-specific MMU8 and 12 signals suggests that either homolog pairing at these regions is delayed relative to the rest of the chromosome or that completion of regional homolog pairing may require SCP3 and the AE. Finally, these data are in agreement with the assumption that chromosome pairing is restricted to homologs during zygotene/early pachytene (Moses *et al.*, 1984).

Central Element-like SC Structures Form in the Absence of the AE

Chromosome painting in spreads as well as 3D fluorescence imaging showed SCP1 fibers between homologously paired regions (see above). When we investigated sectioned *Sycp3*$^{-/-}$ spermatocyte nuclei at the EM level, we noted the formation of SC-like central element structures with the chromatin along these SCP3-deficient central regions being well structured, engendering a beads-on-a-string pattern (Figure 6, E and F). These SC-like structures lack AEs and closely resemble the central region of wild-type SCs (Figure 6E). Together, these results (Figures 4 and 6, E and F) provide strong evidence that transverse filament proteins are able to stably connect homologous chromatin in homologs in the absence of the AE.

DISCUSSION

Disruption of the AE has dire consequences for the process of synapsis (Roeder, 1997, Zickler and Kleckner, 1999). Here, we observed that deletion of the *Sycp3* AE protein gene leads to absence of AEs at the ultrastructural level, which elicits spermatocyte death at the end of an extended zygotene stage (Yuan *et al.*, 2000). Female meiosis in *Sycp3*$^{-/-}$ mice seems to be more tolerant toward the absence of AEs, because in *Sycp3*$^{-/-}$ oocytes chromosomes fail to condense and to integrate SCP2 into SCP1-positive fibers. Still they pass first meiotic prophase, but small chromosomes often undergo nondisjunction (Yuan *et al.*, 2002).

SCP3-deficent Telomeres Attach via a Flat Disk-shape Plate to the Inner Nuclear Membrane

AEs make intimate contact to the NE with the wide end of a conical thickening (Woollam *et al.*, 1966; Esponda and Giménez-Martín, 1972; Holm and Rasmussen, 1977). Tight tethering of meiotic telomeres to the NE may reflect the mechanical requirements for telomere movements along the NE

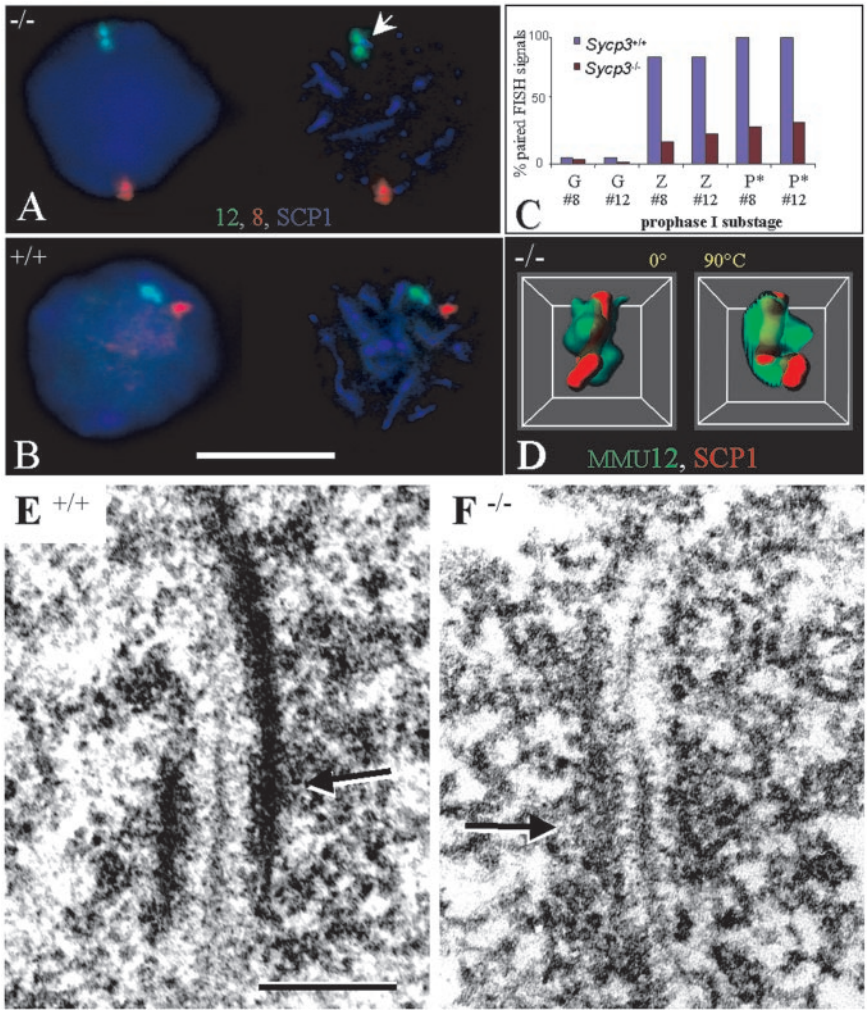

Figure 6. Homolog pairing in *Sycp3*$^{-/-}$ and wild-type (*Sycp3*$^{+/+}$) spermatocytes detected by FISH with MMU8 (red, Cy3) and 12 (green, FITC) region-specific DNA probes in combination with IF for SCP1 (blue, Cy5, false colored). (A) *Sycp3*$^{-/-}$ nucleus (DNA blue, left detail) with paired MMU8 and MMU12 signals (focal plane near the nuclear equator). Paired MMU12 signals (arrow) colocalize with a SCP1 fiber fragment signal (blue, right detail) (arrow). (B) Wild-type spermatocyte with paired MMU8 and MMU12 signals (focal plane near the nuclear equator). SCP1 fibers (blue) and FISH signals of the same nucleus are shown to the right. Bar (A), 10 μm, it applies to A and B. (C) Frequencies of pairing of homologous MMU8 and 12 signals in spermatogonia (G), zygotene (Z), and pachytene nuclei (P*); the asterisk refers to *Sycp3*$^{-/-}$ spermatocyte nuclei with long SCP1 fibers. In round spermatogonia homologous signal pairing occur red in ≤10% of *Sycp3*$^{-/-}$ and WT nuclei (n = 56 and 48, respectively). Zygotene spermatocytes: pairing of MMU8 or 12 homologous regions is seen in 84% of wild-type nuclei, but only in 17 and 23% of *Sycp3*$^{-/-}$ nuclei (n = 31 and 74, respectively). Pairing is reduced but not abolished in advanced *Sycp3*$^{-/-}$ zygotene nuclei (P*; n = 86). P* equals pachytene in the wild-type. (D) 3D reconstruction of a deconvoluted nuclear region of a *Sycp3*$^{-/-}$ spermatocyte that shows a SCP1 core (red) surrounded by paired MMU12-specific chromatin (green; FISH). Two angles (0° and 90°) of the same region are shown after computational rotation. Wild-type SCP1/MMU12 chromatin associations were similar (our unpublished data). (E) EM of a detail of a sectioned wild-type spermatocyte showing tripartite SC with transverse filaments connecting electron-dense lateral elements (arrow). Note the central element. (F) EM of a detail of a *Sycp3*$^{-/-}$ spermatocyte I showing a succession of transverse filaments forming a central element. A row of ordered chromatin grains follows the course of this central region-like structure (arrow) giving raise to a delicate SC-like structure. Bar (E), 0.2 μm, and it also applies to F.

(Alsheimer *et al*., 1999) and may also mask the meiotic chromosome end efficiently from the checkpoint machinery that monitors DSB occurrence and repair during meiosis.

Meiotic telomeres of *Sycp3*$^{-/-}$ spermatocytes lack the conical thickening at the AE end, which uncovered that telomeres attach to the inner nuclear membrane through a flat, disk-shaped attachment plate. This reveals SCP3 to be the major structural determinant of the conical end knob of the axial/lateral element at the inner NM. Our results provide strong evidence that telomere attachment to the meiotic nuclear envelope does not require AE assembly.

EM in situ DNA labeling and telomere EM-ISH showed that the telomere attachment plate contains T_2AG_3 telomere repeats. This provides evidence that telomere repeats are involved in linking the meiotic telomere to the inner nuclear membrane, whereas SCP3 is dispensable for this process. The presence of TRF1 and TRF2 and mammalian Rap1 telomere proteins at perinuclear *Sycp3*$^{-/-}$ telomeres indicates the presence of a wild-type telomere complex in AE-deficient meiotic chromosomes. Previously, it has been proposed that mammalian TRF telomere binding proteins could be required for tethering telomere repeats to the attachment plaque (Scherthan *et al*., 2000a). Although we noted an extension of meiotic chromosome territories, telomeric FISH signals remained the same size in the absence of SCP3, suggesting that other factors than SC proteins dictate the compaction of telomere DNA at meiosis (see below). Significantly smaller T_2AG_3 DNA loops have been observed at meiotic telomeres (Heng *et al*., 1996), which could reflect the compact packaging of these repeats into the dense attachment plate at the meiotic chromosome end. It is conceivable that a telomere binding protein, or, in analogy to the situation in *S. pombe*, a TRF-associated protein such as Rap1 could mediate tethering of meiotic telomeres to the NE. This would agree with the cup-like localization of MTBP, a TRF2-related telomere-binding protein at nuclear envelopes of frog oocytes (Podgornaya *et al*., 2000).

The presence of telomere repeats at NE attachment plates of meiotic chromosomes aligns with previous evidence, especially in yeast, that telomere repeats and associated proteins are imperative for linking meiotic chromosome ends to the nuclear envelope (Rockmill and Roeder, 1998; Trelles-Sticken *et al*., 2000; Chikashige and Hiraoka, 2001, Kanoh and Ishikawa, 2001; Maddar *et al*., 2001).

Cohesion at Meiotic Telomeres

Our IF experiments on the *Sycp3*$^{-/-}$ telomere complex also revealed a telomere protein/SCP2 colocalization. SCP2 in turn interacts with SMC1/3 cohesin proteins (Eijpe *et al*., 2000). Because we noted a reduction of telomere signal number (but not centromere number) to the haploid in advanced *Sycp3*$^{-/-}$ spermatocytes and because the telomere signals colocalized with SCP2 and the meiotic STAG3 cohesin, it seems that telomere–telomere interactions may be mediated by some sort of cohesion. Aside from meiotic cohesins/SCP2, it is also conceivable that the observed pairing of telomere signals could be due to T_2AG_3 repeat-associated proteins themselves, because TRF1 and TIN2 have been shown to mediate pairing of telomeric sequence tracks in vitro (Griffith *et al*., 1998; Kim *et al*., 2003) and fiber-like telomere protein fibers have been observed between mammalian meiotic telomeres (Scherthan *et al*., 2000a). Stickiness of meiotic telomeres may have the potential to slow telomere movements during their clustering in the bouquet stage.

The quality of telomere pairing interactions, however, seems to be distinct from synapsis, because SCP1 generally failed to colocalize with meiotic telomeres and their proteins. This resembles the situation in *Caenorhabditis elegans* where telomeres display a synapsis-independent capacity of pairing (MacQueen *et al*., 2002). Furthermore, telomere cohesion may serve additional functions, because the SC dissolves during diplotene, whereas the telomere complex remains prominent. At MI the telomere is the latest point of release of sister chromatid cohesion, at least in insects (Suja *et al*., 1999; LaFountain *et al*., 2002).

Bouquet Stage Duration Is Extended in the Absence of AEs

Homologous (and heterologous) telomeres get in tight contact during the bouquet stage (Scherthan, 2001), well after cohesin axes have been formed (Prieto *et al*., 2001; Eijpe *et al*., 2003). In the male mouse, this telomere clustering is extremely short, leaving only a few bouquet stage cells detectable (Scherthan *et al*., 1996). FISH with telomere and major satellite probes showed that initiation of first meiotic prophase, as measured by the occurrence of midpreleptotene nuclei, occurs at the same rate in WT and *Sycp3*$^{-/-}$ spermatogenesis. In more advanced *Sycp3*$^{-/-}$ spermatocytes, meiotic chromosome dynamics were altered such that nuclei with clustered telomeres accumulated nearly threefold, which suggests that this transitory stage at the leptotene/zygotene transition be extended in the absence of SCP3/AEs. This agrees with our presumption that bouquet formation is triggered early in meiosis and implies a role of *Sycp3* and the AE in the resolution of the bouquet stage, which could be mediated through several mechanisms (see below).

The distribution of recombination proteins such as Rad51 and RPA is altered in *Sycp3*$^{-/-}$ spermatocytes (Yuan *et al*., 2000), and distorted crossover distribution and extended SC length has been observed in *Sycp3*$^{-/-}$ oocytes (Yuan *et al*., 2002). Defects in recombination have been shown to extend the duration of the bouquet stage in mutants from various kingdoms that are defective in initiation or completion of meiotic double strand break (DSB) repair and synapsis (Pandita *et al*., 1999; Trelles-Sticken *et al*., 1999; Mikhailova *et al*., 2001; Golubovskaya *et al*., 2002; Bass *et al*., 2003). Recently, it has been found that the knockout mouse for the histone 2 variant H2AX displays a significantly extended bouquet stage, although chromosomes synapse and autosome condensation is normal (Fernandez-Capetillo *et al*., 2003; Liebe and Scherthan, unpublished data). The lower frequencies of bouquet stage nuclei in *Sycp3*$^{-/-}$ spermatogenesis compared with *H2ax*$^{-/-}$ and *Atm*$^{-/-}$ spermatogenesis (Pandita *et al*., 1999; Fernandez-Capetillo *et al*., 2003) suggests that SCP3, and by inference the AE, may not directly be involved in control of bouquet exit, because *Atm*$^{-/-}$ spermatocytes die during the same stage but accumulate bouquet stage nuclei (Scherthan *et al.* 2000b) >20-fold over *Sycp3*$^{-/-}$ spermatogenesis. The latter observation also excludes that the relatively mild accumulation of bouquet stage nuclei in *Sycp3*$^{-/-}$ relative to *Atm*$^{-/-}$ spermatogenesis could be due to apoptosis of *Sycp3*$^{-/-}$ spermatocytes; in both mutants spermatocytes I die during an extended zygotene-like stage. This suggests that there are more players in the regulation of bouquet stage duration yet to be discovered in mammals (see below).

SCP3 Is Required for Meiotic Chromosome Condensation

It has been assumed that the resolution of meiotic telomere clustering is passively driven by chromosome condensation (Scherthan *et al*., 1996). In agreement, the bouquet stage lasts longer in oocytes (Pfeifer *et al*., 2003) whose chromosomes and SCs are more extended relative to the male (Barlow and Hultén, 1997; Pfeifer *et al*., 2003). Chromosome painting has now shown that MMU13 bivalents in advanced *Sycp3*$^{-/-}$ spermatocytes are twofold elongated, which suggests that meiotic chromosome structure is altered in the absence of the AE/LE such that condensational forces along meiotic chromosomes may be weak or absent. This and the observation that the female AEs stain more faintly with SCP3 antisera than male AEs (Barlow and Hultén, 1997; Pfeifer *et al*., 2003) implies SCP3 in mediating condensation of meiotic chromosome cores. A reduction of condensation would also be consistent with an extended bouquet stage, although the effect is difficult to tease apart from the impact of potentially derailed DSB repair in the *Sycp3* knockout. It will thus be interesting to learn about bouquet duration in mutants that contain relaxed or hypercondensed meiotic chromosomes and in mutants without DSB repair such as the *Spo11* knockout.

Sycp3$^{-/-}$ *Spermatocytes Undergo Homolog Interactions*

Reduced but significant levels of FISH signal pairing at internal MMU8 and 12 loci and of painted chromosomes 13 suggest that the absence of SCP3/AEs does not abolish the capacity of homolog recognition and pairing. Colocalization of SCP1 signals with paired chromosome 8- and 12-specific signals and the presence of SCP1 fiber fragments in painted MMU13 bivalents (Figure 4F) suggests that SCP1 can connect homologous sequences in the absence of AEs. EM analysis of *Sycp3*$^{-/-}$ spermatocytes suggests that it does so by interconnecting homologous chromatin by assembly striated transverse filament structures, which resemble the central element of the SC. These connections argue against a role of the AE in establishing homolog interactions or in anchoring transverse filaments. Furthermore, nonhomologous synapsis is thought to occur late in pachytene (Moses *et al*., 1984), a stage that is not reached by *Sycp3*$^{-/-}$ spermatocytes. Homologous signal pairing in the absence of SCP1 fibers suggests that the potential for homolog recognition and pairing is not compromised in SCP3/AE-deficient spermatocytes, which agrees with homologue pairing in *Sycp3*$^{-/-}$ females (Yuan *et al*., 2002). Homolog pairing in the absence of SCP1 fibers mimics the situation in the *zip1* mutant of yeast (Sym *et al*., 1993) where it occurs without synapsis (Rockmill *et al*., 1995; Nag *et al*., 1995). Our findings thus

predict homolog pairing to occur in a yet-to-generate *Sycp1* knockout mouse.

Different rates of stable pairing at telomeric and interstitial chromosome regions in the male *Sycp3*$^{-/-}$ mouse suggests that homolog pairing and telomere clustering may be processes that follow different rules. This interpretation agrees with delayed but faithful chromosome pairing in the *ndj1* bouquet mutant of budding yeast that lacks telomere attachment and clustering (Trelles-Sticken *et al*., 2000). Together, it seems that the SCP3 protein is a major structural component of meiotic chromosome cores providing a solid framework for the coordination of telomere and chromosome movements with homolog pairing and meiotic DNA repair.

ACKNOWLEDGMENTS

We are grateful to Jian Guo Liu for providing the *Sycp3*-null testes. We thank C. Heyting (Wageningen, The Netherlands), J.L. Barbero (Madrid, Spain), P. Moens (York, Canada); and T. de Lange (Rockefeller University, New York City) for help with the antibodies and D.C. Ward (Yale University, New Haven, CT) for mouse probes. H.S. acknowledges support from the DFG (SCHE 350/8-4) and from H.H. Ropers (Max Planck Institute for Molecular Genetics, Berlin, Germany). C.H. received support from the Swedish Research Council and the Swedish Cancer Society. R.B. received support from the DFG (Be 1168/4-4) and the Graduiertenkolleg 639.

REFERENCES

Alsheimer, M., and Benavente, R. (1996). Change of karyoskeleton during mammalian spermatogenesis: expression pattern of nuclear lamin C2 and its regulation. Exp. Cell Res. *228*, 181–188.

Alsheimer, M., von Glasenapp, E., Hock, R., and Benavente, R. (1999). Architecture of the nuclear periphery of rat pachytene spermatocytes: distribution of nuclear envelope proteins in relation to synaptonemal complex attachment sites. Mol. Biol. Cell *10*, 1235–1245.

Barlow, A.L., and Hultén, M.A. (1997). Combined immunocytogenetic and molecular cytogenetic analysis of meiosis I oocytes from normal human females. Zygote *6*, 27–38.

Bass, H.W., Bordoli, S.J., and Foss, E.M. (2003). The desynaptic (dy) and desynaptic1 (*dsy1*) mutations in maize (*Zea mays* L.) cause distinct telomere-misplacement phenotypes during meiotic prophase. J. Exp. Bot. *54*, 39–46.

Benavente, R., Alsheimer, M., and von Glasenapp, E. (2004). The nuclear envelope at the attachment sites of mammalian meiotic telomeres. Chrom. Today *14* (*in press*).

Bojko, M. (1990). Synaptic adjustment of inversion loops in *Neurospora crassa*. Genetics *124*, 593–598.

Broccoli, D., Smogorzewska, A., Chong, L., and de Lange, T. (1997). Human telomeres contain two distinct Myb-related proteins, TRF1 and TRF2. Nat. Genet. *17*, 231–235.

Buonomo, S.B., Clyne, R.K., Fuchs, J. Loidl, J. Uhlmann, F., and Nasmyth, K. (2000). Disjunction of homologous chromosomes in meiosis I depends on proteolytic cleavage of the meiotic cohesin Rec8 by separin. Cell *103*, 387–398.

Boyle, A.L., and Ward, D.C. (1992). Isolation and initial characterization of a large repeat sequence element specific to mouse chromosome 8. Genomics *12*, 517–525.

Chikashige, Y., and Hiraoka, Y. (2001). Telomere binding of the Rap1 protein is required for meiosis in fission yeast. Curr. Biol. *11*, 1618–1623.

Cooper, J.P., Watanabe, Y., and Nurse, P. (1998) Fission yeast Taz1 protein is required for meiotic telomere clustering and recombination. Nature *392*, 828–831.

de Lange, T. (2002). Protection of mammalian telomeres. Oncogene *21*, 532–540.

Dresser, M.E., and Moses, M.J. (1980). Synaptonemal complex karyotyping in spermatocytes of the chinese hamster *Cricetulus griseus*: IV. Light and electron microscopy of synapsis and nuclear development by silver staining. Chromosoma *76*, 1–22.

Eijpe, M., Heyting, C., Gross, B., and Jessberger, R. (2000). Association of mammalian SMC1 and SMC3 proteins with meiotic chromosomes and synaptonemal complexes. J. Cell Sci. *113*, 673–682.

Eijpe, M., Offenberg, H., Jessberger, R., Revenkova, E., and Heyting, C. (2003). Meiotic cohesin REC8 marks the axial elements of rat synaptonemal complexes before cohesins SMC1beta and SMC3. J. Cell Biol. *160*, 657–670.

Esponda, P., and Giménez-Martín, G. (1972). The attachment of the synaptonemal complex to the nuclear envelope. An ultrastructural and cytochemical analysis. Chromosoma *38*, 405–417.

Fernandez-Capetillo, O., Liebe, B., Scherthan, H., and Nussenzweig, A. (2003). H2AX regulates meiotic telomere clustering. J. Cell Biol. *163*, 15–20.

Franco, S., Alsheimer, M., Herrera, E., Benavente, R., and Blasco, M. (2002). Mammalian meiotic telomeres: composition and ultrastructure in telomerase deficient mice. Eur. J. Cell Biol, *81*, 335–340.

Golubovskaya, I.N., Harper, L.C., Pawlowski, W.P., Schichnes, D., and Cande, W.Z. (2002). The *pam1* gene is required for meiotic bouquet formation and efficient homologous synapsis in maize (*Zea mays* L.). Genetics *162*, 1979–1993.

Griffith, J., Bianchi, A., and de Lange, T. (1998). TRF1 promotes parallel pairing of telomeric tracts in vitro. J. Mol. Biol. *278*, 79–88.

Heng, H.H.Q., Chamberlain, J.W., Shi, X.M., Spyropoulos, B., Tsui, L.C., and Moens, P.B. (1996). Regulation of meiotic chromatin loop size by chromosomal position. Proc. Natl. Acad. Sci. USA *93*, 2795–2800.

Holm, P.B. (1977). 3 dimensional reconstruction of chromosome pairing during the zygotene stage of meiosis in *Lilium longiflorum*. Carlsberg Res. Commun. *42*, 103–152.

Holm, P.B., and Rasmussen, S.W. (1977). Human meiosis I. The human pachytene karyotype analyzed by three-dimensional reconstruction of the synaptonemal complex. Carlsberg Res. Commun. *24*, 283–323.

Hunter, N. (2003). Synaptonemal complexities and commonalities. Mol. Cell *12*, 533–535.

Kim, S.H., Han, S., You, Y.H., Chen, D.J., and Campisi, J. (2003). The human telomere-associated protein TIN2 stimulates interactions between telomeric DNA tracts in vitro. EMBO Rep. *4*, 685–691.

Kanoh, J., and Ishikawa, F. (2001). spRap1 and spRif1, recruited to telomeres by Taz1, are essential for telomere function in fission yeast. Curr. Biol. *11*, 1624–1630.

Klein, F., Mahr, P., Galova, M., Buonomo, S.B., Michaelis, C., Nairz, K., and Nasmyth, K. (1999). A central role for cohesins in sister chromatid cohesion, formation of axial elements, and recombination during yeast meiosis. Cell *98*, 91–103.

LaFountain, J.R. Jr., Cole, R.W., and Rieder, C.L. (2002). Partner telomeres during anaphase in crane-fly spermatocytes are connected by an elastic tether that exerts a backward force and resists poleward motion. J. Cell Sci. *115*, 1541–1549.

Lammers, J.H.M., Offenberg, H.H., van Aalderen, M., Vink, A.C.G., Dietrich, A.J.J., and Heyting, C. (1994). The gene encoding a major component of the lateral elements of synapto-nemal complexes of the rat is related to X-linked lymphocyte-regulated genes. Mol. Cell. Biol. *14*, 1137–1146.

Lee, J.Y., and Orr-Weaver, T.L. (2001). The molecular basis of sister-chromatid cohesion. Annu. Rev. Cell Dev. Biol. *17*, 753–777.

Li, B., Oestreich, S., and de Lange, T. (2000). Identification of human Rap *1*: implications for telomere evolution. Cell *101*, 471–483.

Liu, J.G., Yuan, L., Brundell, E., Björkroth, B., Daneholt, B., and Höög, C. (1996). Localization of the N-terminus of SCP1 to the central element of the synaptonemal complex and evidence for direct interactions between the N-termini of SCP1 molecules organized head-to-head. Exp. Cell Res. *226*, 11–19.

Loidl, J. (1990). The initiation of meiotic chromosome pairing: the cytological view. Genome *33*, 759–778.

MacQueen, A.J., Colaiacovo, M.P., McDonald, K., and Villeneuve, A.M. (2002). Synapsis-dependent and -independent mechanisms stabilize homolog pairing during meiotic prophase in *C. elegans*. Genes Dev. *16*, 2428–2442.

Maddar, H., Ratzkovsky, N., and Krauskopf, A. (2001). Role for telomere cap structure in meiosis. Mol. Biol. Cell *12*, 3191–3203.

McEachern, M.J., Krauskopf, A., and Blackburn, E.H. (2000). Telomeres and their control. Annu. Rev. Genet. *34*, 331–358.

Meuwissen, R.L., Offenberg, H.H., Dietrich, A.J., Riesewijk, A., van Iersel, M., and Heyting, C. (1992). A coiled-coil related protein specific for synapsed regions of meiotic prophase chromosomes. EMBO J. *11*, 5091–100.

Mikhailova, E.I., Sosnikhina, S.P., Kirillova, G.A., Tikholiz, O.A., Smirnov, V.G., Jones, R.N., and Jenkins, G. (2001). Nuclear dispositions of subtelomeric and pericentromeric chromosomal domains during meiosis in asynaptic mutants of rye (*Secale cereale* L.). J. Cell Sci. *114*, 1875–1882.

Moens, P.B. (1995). Histones H1 and H4 of surface-spread meiotic chromosomes. Chromosoma *104*, 169–174.

Moens, P.B. (1969). The fine structure of meiotic chromosome polarization and pairing in *Locusta migratoria* spermatocytes. Chromosoma *28*, 1–25.

Molnar, M., Bahler, J., Sipiczki, M., and Kohli, J. (1995). The rec8 gene of *Schizosaccharomyces pombe* is involved in linear element formation, chromosome pairing and sister-chromatid cohesion during meiosis. Genetics *141*, 61–73.

Moses, M.J., Dresser, M.E., and Poorman, P.A. (1984). Composition and role of the synaptonemal complex. Symp. Soc. Exp. Biol. *38*, 245–270.

Nag, D.K., Scherthan, H., Rockmill, B., Barghava, J., and Roeder, G.S. (1995). Heteroduplex DNA formation and homolog pairing in yeast meiotic mutants. Genetics *141*, 75–86.

Naito, T., Matsuura, A., and Ishikawa, F. (1998). Circular chromosome formation in a fission yeast mutant defective in two ATM homologues. Nat. Genet. *20*, 203–206.

Nimmo, E.R., Pidoux, A.L., Perry, P.E. and Allshire, R.C. (1998). Defective meiosis in telomere-silencing mutants of *Schizosaccharomyces pombe.* Nature *392*, 825–828.

Offenberg, H.H., Schalk, J.A.C., Meuwissen, R.L.J., van Aalderen, M., Kester, H.A., Dietrich, A.J.J., and Heyting, C. (1998). SCP *2*, a major protein component of the axial elements of synaptonemal complexes of the rat. Nucleic Acid Res. *26*, 2572–2579.

Pandita, T.K., Westphal, C.H., Anger, M., Sawant, S.G., Geard, C.R., Pandita, R.K., and Scherthan, H. (1999). Atm inactivation results in aberrant telomere clustering during meiotic prophase. Mol. Cell. Biol. *19*, 5096–5105.

Pelttari, J., *et al*. (2001). A meiotic chromosomal core consisting of cohesin complex proteins recruits DNA recombination proteins and promotes synapsis in the absence of an axial element in mammalian meiotic cells. Mol. Cell. Biol. *21*, 5667–5677.

Peters, A.H., Plug, A.W., van Vugt, M.J., and de Boer, P. (1997). A drying-down technique for the spreading of mammalian meiocytes from the male and female germline. Chromosome Res. *5*, 66–68.

Petronczki, M., Siomos, M.F., and Nasmyth, K. (2003). Un menage a quatre: the molecular biology of chromosome segregation in meiosis. Cell *112*, 423–440.

Pezzi, N., Prieto, L., Kremer, L., Perez Jurado, L.A., Valero, C., Del Maso, J., Martinez, A.C., and Barbero, J.L. (2000). STAG3, a novel gene encoding a protein involved in meiotic chromosome pairing and location of STAG3-related genes flanking the Williams-Beuren syndrome deletion. FASEB J. *14*, 581–592.

Pfeifer, C., Scherthan, H., and Thomsen, P.D. (2003). Sex-specific telomere redistribution and synapsis initiation in cattle oogenesis. Dev. Biol. *255*, 206–215.

Podgornaya, O.I., Bugaeva, E.A., Voronin, A.P., Gilson, E., and Mitchell, A.R. (2000). Nuclear envelope associated protein that binds telomeric DNAs. Reprod. Dev. *57*, 16–25.

Prieto, I., Suja, J.A., Pezzi, N., Kremer, L., Martinez, A., Rufas, J.S., and Barbero, J.L. (2001). Mammalian STAG3 is a cohesin specific to sister chromatid arms in meiosis I. Nat. Cell Biol. *3*, 761–766.

Revenkova, E., Eijpe, M., Heyting, C., Gross, B., and Jessberger, R. (2001). Novel meiosis-specific isoform of mammalian SMC1. Mol. Cell. Biol. *21*, 6984–6998.

Rockmill, B., and G.S. Roeder. (1998). Telomere-mediated chromosome pairing during meiosis in budding yeast. Genes Dev. *12*, 2574–2586.

Rockmill, B., Sym, M., Scherthan, H., and Roeder, G.S. (1995). Roles for two RecA homologs in promoting meiotic chromosome synapsis. Genes Dev. *9*, 2684–2695.

Roeder, G.S. (1997). Meiotic chromosomes: it takes two to tango. Genes Dev. *11*, 2600–2621.

Scherthan, H. (2001). A bouquet makes ends meet. Nat. Rev. Mol. Cell. Biol. *2*, 621–627.

Scherthan, H., and Schönborn, I. (2001). Asynchronous chromosome pairing in male meiosis of the rat (*Rattus norvegicus*). Chromosome Res. *9*, 273–282.

Scherthan, H., Jerratsch, M., Li, B., Smith, S., Hultén, M., Lock, T., and de Lange, T. (2000a). Mammalian meiotic telomeres: protein composition and their redistribution in relation to nuclear pores. Mol. Biol. Cell *11*, 4189–4203.

Scherthan, H., *et al*. (2000b). Meiotic telomere distribution and Sertoli cell nuclear architecture is altered in Atm- and Atm/p53-deficient mice. Mol. Cell. Biol. *20*, 7773–7783.

Scherthan, H., Weich, S., Schwegler, H., Heyting, C., Härle, M., and Cremer, T. (1996). Centromere and telomere movements during early meiotic prophase of mouse and man are associated with the onset of chromosome pairing. J. Cell Biol. *134*, 1109–1125.

Stack, S.M. (1984). Heterochromatin, the synaptonemal complex and crossing over. J. Cell Sci. *71*, 159–176.

Steinmüller, J., Schleiermacher, E., and Scherthan, H. (1993). Direct detection of repetitive, whole chromosome paint and telomere DNA probes by immunogold electron microscopy. Chromosome Res. *1*, 45–51.

Suja, J.A., Antonio, C., Debec, A., and Rufas, J.S. (1999). Phosphorylated proteins are involved in sister-chromatid arm cohesion during meiosis I. J. Cell Sci. *112*, 2957–2969.

Sym, M., J. Engebrecht, and G. S. Roeder. (1993). ZIP1 is a synaptonemal complex protein required for meiotic chromosome synapsis. Cell *72*, 365–378.

Thiry, M. (1992). Highly sensitive immunodetection of DNA on sections with exogenous terminal deoxynucleotidyl transferase and non-isotopic nucleotide analogs. J. Histochem. Cytochem. *40*, 411–419.

Trelles-Sticken, E., Dresser, M.E., and Scherthan, H. (2000). Meiotic telomere protein Ndj1p is required for meiosis-specific telomere distribution, bouquet formation and efficient homologue pairing. J. Cell Biol. *151*, 95–106.

Trelles-Sticken, E., Loidl, J., and Scherthan, H. (1999). Bouquet formation in budding yeast: initiation of recombination is not required for meiotic telomere clustering. J. Cell Sci. *112*, 651–658.

von Wettstein, D., Rasmussen, S.W., and Holm, P.B. (1984). The synaptonemal complex in genetic segregation. Annu. Rev. Genet. *18*, 331–413.

Watanabe, Y., and Nurse, P. (1999). Cohesin Rec8 is required for reductional chromosome segregation at meiosis. Nature *400*, 461–464.

Woollam, D.H., Ford, E.H., and Millen, J.W. (1966). The attachment of pachytene chromosomes to the nuclear membrane in mammalian spermatocytes. Exp. Cell Res. *42*, 657–661.

Yuan, L., Liu, J.G., Hoja, M.R., Wilbertz, J., Nordqvist, K., and Hoog, C. (2002). Female germ cell aneuploidy and embryo death in mice lacking the meiosis-specific protein SCP3. Science *296*, 1115–1118.

Yuan, L., Liu, J.G., Zhao, J., Brundell, E., Daneholt, B., and Hoog, C. (2000). The murine SCP3 gene is required for synaptonemal complex assembly, chromosome synapsis, and male fertility. Mol. Cell *5*, 73–83.

Yuan, L., Pelttari, J., Brundell, E., Bjorkroth, B., Zhao, J., Liu, J.G., Brismar, H., Daneholt, B., and Hoog, C. (1998). The synaptonemal complex protein SCP3 can form multistranded, cross-striated fibers in vivo. J. Cell Biol. *142*, 331–339.

Zhu, X.D., Kuster, B., Mann, M., Petrini, J.H., and Lange, T. (2000). Cell-cycle-regulated association of AD50/MRE11/NBS1 with TRF2 and human telomeres. Nat Genet. *25*, 347–352.

Zickler, D., and Kleckner, N. (1998). The leptotene-zygotene transition of meiosis. Annu. Rev. Genet. *32*, 619–697.

Zickler, D., and Kieckner, N. (1999). Meiotic chromosomes. Integrating structure and function. Annu. Rev. Genet. *33*, 603–754.